JCTC Journal of Chemical Theory and Computation

Theoretical Study of the Reaction Mechanism of *Streptomyces coelicolor* Type II Dehydroquinase

L. Mattias Blomberg,*,† Martina Mangold,‡ John B. O. Mitchell,† and Jochen Blumberger*,‡

Unilever Centre for Molecular Science Informatics, Department of Chemistry, University of Cambridge, Lensfield Road, Cambridge, CB2 1EW, U.K.

Received November 7, 2008

Abstract: The reaction mechanism of a type II dehydroquinase (DHQase) from *Streptomyces coelicolor* was investigated using molecular dynamics simulation and density functional theory (DFT) calculations. DHQase catalyzes the elimination of a water molecule from dehydroquinate (DHQ), a key step in the biosynthesis of aromatic amino acids in bacteria, fungi, and plants. In the DFT calculations, 10 models, containing up to 230 atoms, were used to investigate different proposals for the reaction mechanism, suggested on the basis of crystal structures and kinetic data. Probing the flexibility of the active site, molecular dynamics simulation reveals that deprotonated Tyr28 can act as the base that catalyzes the first reaction step, the proton abstraction of the *pro-S* proton at C2 of DHQ, and formation of the enolate intermediate. The computed barrier for the first transition state (TS1), 13−15 kcal/mol, is only slightly affected by the active site model used and is in good agreement with the corresponding experimental barrier of 13.4 kcal/mol for the rate-determining step. The previously proposed enol form of the intermediate is found to be significantly higher in energy than the enolate form and is thus thermodynamically not competitive. In the second and final reaction step, protonation of the hydroxyl group at C1 by His106 followed by water elimination, there is a substantial buildup of dipole moment due to the net transfer of a proton from His106 to Tyr28. A barrier for the second transition state (TS2) that fits well with the corresponding experimental barrier could only be found if the buildup of dipole moment is at least partly compensated during the second reaction step. We speculate that this could be facilitated by regeneration of the Tyr28 anion or by proton transfer to the vicinity of His106 *before* TS2 is reached. A revised mechanism for type II DHQase is discussed in light of the results of the present calculations.

1. Introduction

The shikimate pathway is a biosynthetic route producing among others the aromatic amino acids phenylalanine, tyrosine, and tryptophan.[1−4] Chorismate is the end product of the shikimate pathway and the starting point of the synthesis of these aromatic compounds. The shikimate pathway is present in bacteria, fungi, and plants, but absent in mammals, who have to derive aromatic compounds from their diet. Hence, the shikimate pathway enzymes are attractive targets for herbicides, fungicides, and antibiotics. As an example, we mention the broad-spectrum herbicide glyphosate, an inhibitor of the penultimate step of the shikimate pathway,[5] which is, however, not suitable as an antibiotic.

The third step of the shikimate pathway, the reversible dehydration of 3-dehydroquinate (DHQ) to 3-dehydroshikimate (DHS) catalyzed by 3-dehydroquinate dehydratase, often abbreviated to dehydroquinase (DHQase, E.C. 4.2.1.10), has been an attractive target for recent inhibitor design. There are two types of DHQases, type I and II, and both catalyze

* Corresponding author e-mail: blomberg.mattias@gmail.com; jb376@cam.ac.uk.

† Unilever Centre for Molecular Science Informatics.

‡ Department of Chemistry.

10.1021/ct800480d CCC: $40.75
Published on Web 04/16/2009

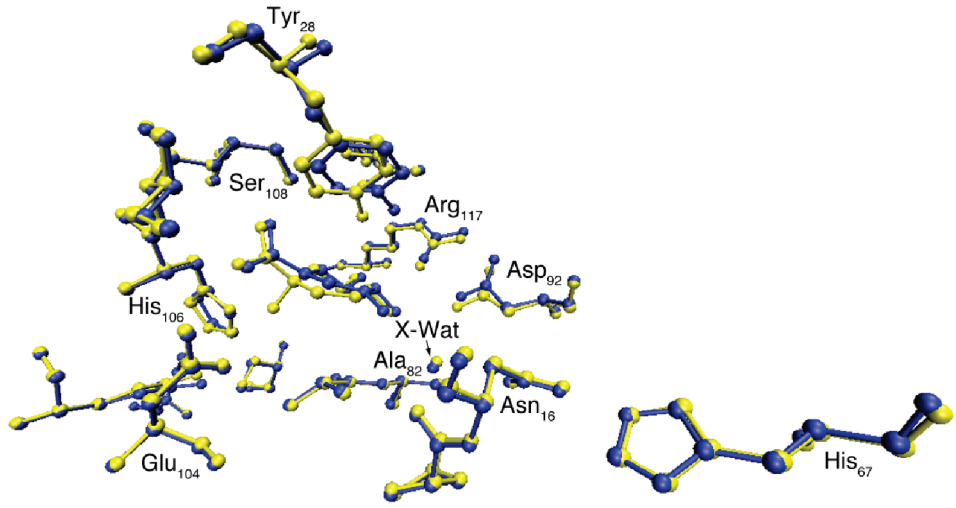

Figure 1. Aligned X-ray structures of DHQase in *S. coelicolor*. The wild-type with 2,3-anhydro-quinic acid bound is in yellow, and the R23A mutant with DHS bound is in blue.[16] The rmsd between the two structures is only 0.15 Å in the active site region.

the same overall reaction but are structurally unrelated and use different reaction mechanisms for their catalysis.[6,7] Some bacteria, such as *Escherichia coli* or *Salmonella typhi*, have type I enzymes,[8] whereas other bacteria, such as *Streptomyces coelicolor*,[9] *Mycobacterium tuberculosis*,[10] and *Helicobacter pylori*,[11] have type II enzymes. This type of convergent evolution is very uncommon for enzymes in central metabolic pathways.[12] The type II enzymes catalyze the trans dehydration of 3-dehydroquinate via a proposed enol/enolate intermediate,[13] whereas the type I enzymes catalyze a cis dehydration via an imine intermediate utilizing a conserved lysine residue.[8]

Type II DHQase is a dodecamer consisting of four trimeric units. DHQase from both *S. coelicolor* and *M. tuberculosis* can be dissociated into trimers, which were shown to be catalytically active.[14] The active site in DHQase is located in a cleft at the C-terminal end of the five-stranded parallel β-sheet. The binding pocket is covered by a loop containing residues 21−31. The loop has been shown to be flexible and closed upon binding of the substrate.[15] Furthermore, the active site of a subunit is located close to the interface of a neighboring subunit. The binding conformation of the substrate was revealed in the structures of both the wild-type enzyme forming a complex with the transition-state analogue 2,3-anhydro-quinic acid and also in an inactive R23A mutant, in which the product DHS is bound[16] (Figure 1). The substrate is held in place by about 20 hydrogen bonds. A schematic picture of the hydrogen bond network of the active site is shown in Figure 2.

While several type II DHQase inhibitors have been synthesized with affinities ranging from micromolar to nanomolar,[17−21] the type II reaction mechanism is far from being understood. The results of kinetic isotope studies are not consistent with a concerted E2 mechanism but indicate a stepwise E1cB mechanism involving an enolate intermediate.[13] This work and the analysis of crystal structures of *S. coelicolor* in complexes with a number of ligands (PDB code 1GU1)[22] have led to the proposal of a mechanism of DHQase (Figure 3). Tyr28 is assumed to have an unusually low pK_a due to electrostatic interaction with the neighboring positively charged Arg113 residue. This leads, at least to some extent, to deprotonation at physiological pH, thereby providing the base (tyrosinate) that abstracts the *pro-S* hydrogen on C2 of DHQ. The crystal structure of DHQase from *S. coelicolor* together with the measured kinetic isotope effects of DHQase from *A. nidulans* suggest that the enolate intermediate formed is converted into the enol form through proton transfer from a conserved water molecule. The latter is assumed to be regenerated by proton transfer from the amino group of the side chain of Asn16.[16] In the last step of the elimination reaction, the hydroxyl group on C1 is protonated by His106, which leads to cleavage of the C−O bond and formation of the product.

There are a number of open questions regarding the reaction mechanism described above. Not only is the protonation state of Tyr28 uncertain but also the position of Tyr28 in the crystal structure is rather unfavorable for deprotonation from the C2 atom of the substrate. Moreover, the suggested formation of an enol intermediate requires the transient formation of an anion that is likely to be high in energy (hydroxide or deprotonated side chain of an Asn residue). The formation of an enol intermediate has been invoked to explain the solvent isotope effect in DHQase from *A. nidulans*, which showed that two protons are involved in the rate-limiting step.[13] The first proton would be the one transferred from Asn16 via the crystal water to the enolate form of DHQ. The second proton would be the one transferred from His106 in the elimination step. This also implies that both reaction steps occur at similar rates, since both should be, or at least become, rate limiting for their deuterated species, respectively. However, in the same kinetic isotope study for DHQase from *M. tuberculosis*, the corresponding solvent isotope effect indicates the involvement of only one proton in the rate-limiting step.[13] Thus, there is a discrepancy in the mechanisms comparing the two different species.

In the present theoretical study, we investigate the energetic feasibility of various variants of the E1cB reaction

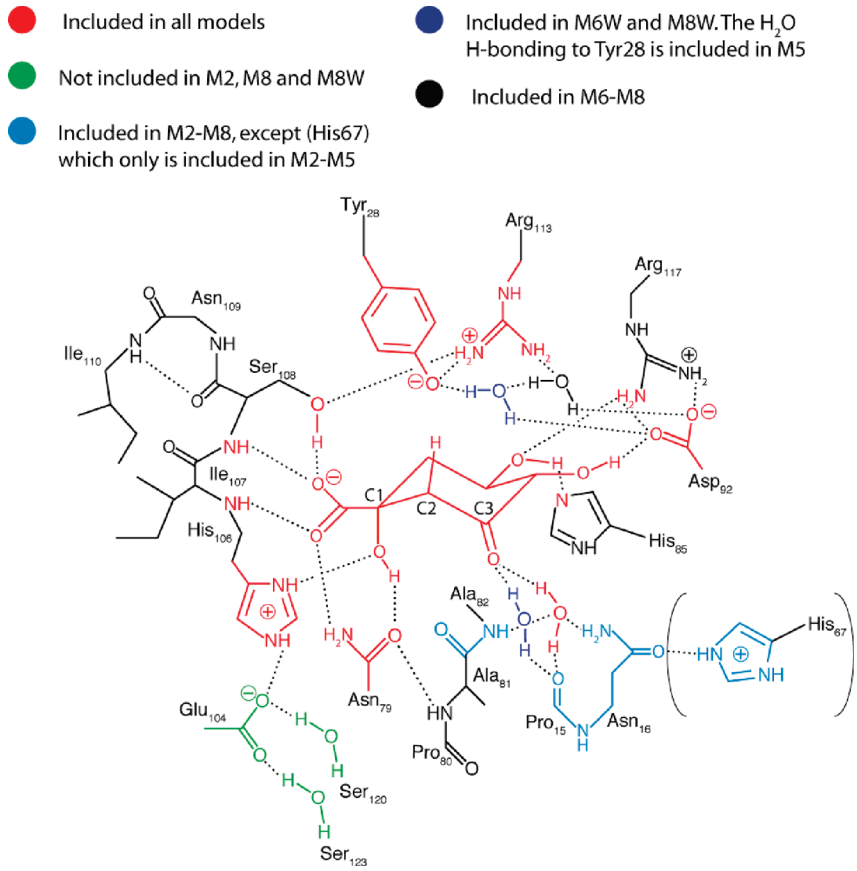

Figure 2. Schematic picture of the active site in DHQase binding the substrate DHQ. The differences in the models used are color coded.

mechanism described above using QM calculations complemented with dynamical information obtained from molecular dynamics simulation of the substrate bound complex. Preliminary investigations on the E2 mechanism showed that the barrier for breaking the C−H and C−OH bonds simultaneously is unfavorable by about 10 kcal/mol, as compared to the E1cB type of mechanism for the corresponding model. This is in line with experimental evidence suggesting that the E2 mechanism does not play an important role.[13] Carrying out long molecular dynamics runs, we find that at room temperature rare thermal fluctuations occasionally bring Tyr28 within hydrogen-bonding distance of the proton at the C2 atom of the substrate. Thus, if Tyr28 is deprotonated, it can function as the base that catalyzes the first reaction step in the E1cB mechanism. The QM calculations show that the deprotonation occurs directly; the water-assisted deprotonation is disfavored by 10 kcal/mol. Moreover, the enol form proposed for the intermediate is found to be too high in energy to compete with the enolate form. The barriers for the reaction steps are obtained in reasonably good agreement with experiment, even though they are rather sensitive to the size of the model used. A revised picture of the reaction mechanism based on the calculations presented herein is given at the end of this article.

2. Methods

2.1. Molecular Dynamics Simulation. We chose a trimeric subunit of DHQase as a model for molecular dynamics simulation. The trimer structure was obtained from the X-ray crystal structure of dodecameric DHQase from (PDB code 1GU1)[22] by selecting chains A, B, and C and the crystal water molecules assigned to them. All three chains were treated as identical. The transition-state analogue 2,3-anhydroquinic acid (AHQ) bound to the active site was modified to DHQ by addition of a carbonyl oxygen atom at C3 and a hydrogen atom at C2. In the crystal structure, two buffer molecules bound in close proximity to the active site (one glycerol molecule and tartaric acid, respectively). They were removed and replaced by nine water molecules. The water molecules were placed so that the oxygen atoms were on top of the crystallographic positions of the oxygen atoms of the two buffer molecules. Two positions for the side chains of Ser30, Glu124, and Glu143 were reported; conformation "A" was taken in this work. In the crystal structure, residues 151−156 were missing; Gly150 was taken as the C-terminus. Hydrogen atoms were added using the program "xleap" included in the AMBER9[37] simulation package. Protonation states of ionizable side chains were chosen corresponding to pH = 7. Tyr28 was modeled in its deprotonated form, histidines 47, 67, 73, and 118 were protonated at the εN atom, histidines 58, 85, 111, and 119 were protonated at the δN atom, and His106 was doubly protonated. The protonation states of the histidine residues were chosen after inspection of the local hydrogen bond network and the extent of exposure to the solvent. The protein was neutralized by adding 21 K^+ ions and solvated by adding 14 753 water molecules and 33 K^+ and Cl^- ions. The molality of KCl was 0.10 mol/kg; the total number of atoms was 52 845.

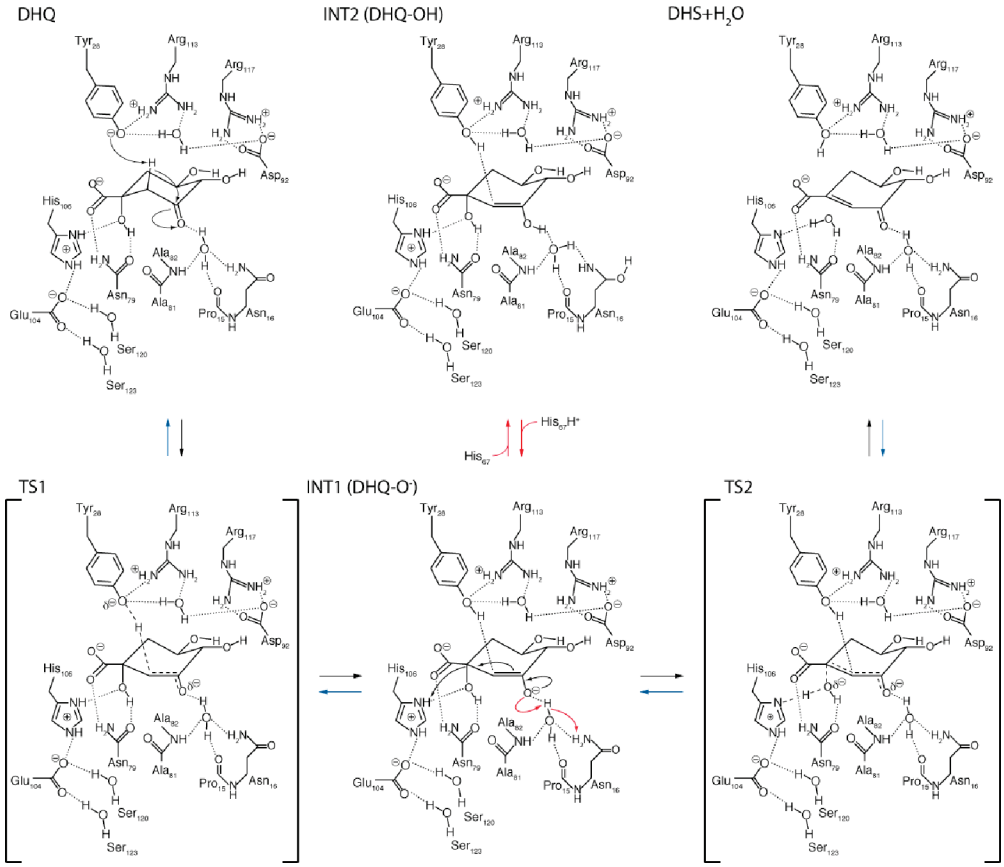

Figure 3. Schematic picture of the proposed reaction mechanism catalyzed by type II DHQase.

The MD simulations were carried out using the AMBER99 force field and the TIP3P model for water. A set of point charges reproducing the electrostatic potential for DHQ and deprotonated Tyr28 was obtained from DFT calculations at the B3LYP/cc-PVTZ(-f)//6-31G(d) IEFPCM (r = 1.4 Å, ε = 4) level of theory. Atomic point charges representing the electrostatic potential from the DFT calculation were obtained according to the RESP method. Force constants for bonds and angles in DHQ were extracted from the Hessian calculated at the B3LYP/6-31G(d)[25,26] level of theory. Seminario's algorithm, which is fully invariant to the choice of internal coordinates,[23] was used to extract force constants for bonds and angles in the optimized structure. The dihedral force constants were taken from the GAFF force field implemented in AMBER.

The atomic positions of DHQ and the nine water molecules replacing the two buffer molecules were relaxed by energy minimization while keeping all protein atoms fixed at their crystallographic positions. All solvent molecules were equilibrated for 50 ps in the NPT ensemble using temperature rescaling to 300 K and a target pressure of 1 bar. Then the protein was equilibrated first by carrying out four consecutive runs of length 100 ps/run using harmonic restraints on the protein atom positions with force constants of 99, 50, 25, and 10 kcal/(mol Å^2). The restraining potentials were removed, and the free protein was equilibrated for 1 ns in the NPT ensemble using a Berendsen thermostat with target temperature 300 K. During this final equilibration period and the subsequent production runs, the center of mass of each of the three subunits was restrained to the value of the crystal structure. The center of mass restraint was applied to avoid tumbling motion of the trimer that would have brought protein atoms too close to the edge of the simulation cell. Using the restraint the smallest distance between any protein atom and the box edge was always larger than 10 Å as compared to the cutoff of 12 Å used for truncation of short-range nonbonded interactions. Production runs used for calculation of thermal averages were carried out for 5 ns in the NVT ensemble using a MD time step of 2 fs. The cell dimensions were 94.03 × 90.34 × 62.69 Å^3. The r-RESPA multiple time stepping method was used with bonded and short-range nonbonded forces calculated every time step and electrostatic forces every second time step. The SPME algorithm[24] with default parameters was used for the latter. All molecular dynamics simulations were carried out with the NAMD[38] package.

2.2. QM Calculations. In the present study, 10 QM models were investigated, each based on the crystal structure of *S. coelicolor*, PDB code 1GU1. The models were chosen so as to investigate different features of the active site and so as to test different propositions regarding the reaction mechanism. The active site in DHQase is large and contained a complex hydrogen-bonding network due to the carboxylate, carbonyl, and the three hydroxyl groups in DHQ (Figure 2). Models M1−M5 focus on modeling the chemically important parts of the active site as accurately as possible, whereas interactions that do not change significantly during the reaction were modeled more approximately. Models M6−M8 are computationally more demanding and incorporate a larger part of the surroundings of the active site. A summary of

Table 1. Differences among Models M1−M8; See Also Figure 2[a]

	M1	M2	M3	M4	M5	M6	M6W	M7	M8	M8W
His67	NM	P	P	NP	P	NM	NM	NM	NM	NM
Glu104	*	NM	*	*	*	*	*	P	NM	NM
Ser120	*	NM	*	*	*	*	*	*	NM	NM
Ser123	*	NM	*	*	*	*	*	*	NM	NM
H_2O[b]	NM	NM	NM	NM	NM	*	*	*	*	*
2 × H_2O[c]	NM	NM	NM	NM	*[d]	NM	*	NM	NM	*

[a] NM - not modeled; * - modeled; P - protonated; NP - not protonated. [b] Water molecule included in models M6−M8, which is hydrogen bonding to $TyrO^-$. [c] Two additional water molecules added in M6W and M8W. One is hydrogen bonding to $TyrO^-$, and the other is hydrogen bonding to the carbonyl oxygen on C3 in DHQ. [d] Note that in M5 only one water is included, which is involved in the proton transfer between DHQ and $TyrO^-$.

the models used is given in Table 1 and Figure 2. Furthermore, a detailed description of the models is given in the Appendix. For all models, the QM region was terminated by saturating the bond that is cut with a hydrogen atom. The latter was positioned along the axis of the bond that is cut at a typical X−H bond length. The reaction energy profile for all model systems was computed using reaction coordinate driving combined with geometry optimization. A small model system (M0) was used for calculation of thermal and entropic contributions to the reaction energies.

The geometries of all the stationary points in the reaction studied were optimized using Becke's[25] three-parameter hybrid exchange functional combined with the Lee−Yang−Parr[26] correlation functional (B3LYP). The calculations were performed using the Gaussian03[27] suite of programs. Geometries and Hessians were obtained using Pople's split valence basis set 6-31G*. Models M1−M5 were optimized taking the dielectric effect of the protein into account by using the integral equation formalism model (IEFPCM) implemented in Gaussian03.[28−30] The dielectric constant was set equal to 4.[31] Bondi's atomic radii were used together with a probe radius of the solvent of 1.4 Å to create a cavity around the solute. Because of their size (∼225 atoms), models M6−M8 were optimized in the gas phase and dielectric effects were included only for the final single point calculations. The final energies for the optimized geometries were evaluated using Pople's triple split valence basis set 6-311+G(2d,2p), containing double polarization on first- and second-row atoms and one diffuse function on second-row atoms. To keep the main features of the structure close to the crystal structure, restrictions on certain atoms were applied during geometry optimization. Either the position of C_α was fixed if included in the model, or the position of the terminating hydrogen atom was fixed. The small rmsd (0.15 Å) between the crystal structure with the transition-state analogue bound and the crystal structure with the product bound (Figure 1) indicates that this restriction on the flexibility of the active site is an adequate approximation for this enzyme. The smallest model (M0) was used for computation of thermal and entropic contributions of the free energy profile. The same corrections were used for all models. The accuracy of the B3LYP functional was tested in the extended G3 benchmark set,[32] which consists of enthalpies of formation, ionization potentials, electron affinities, and proton affinities for molecules containing first- and second-row atoms. In these tests, the B3LYP functional gave an average absolute error of 4.3 kcal/mol for 376 different entries.[32] The calculated enthalpy for the reaction DHQ → DHS + H_2O in aqueous solution was −1.7 kcal/mol, to be compared with the experimental value of 0.6 kcal/mol.[33]

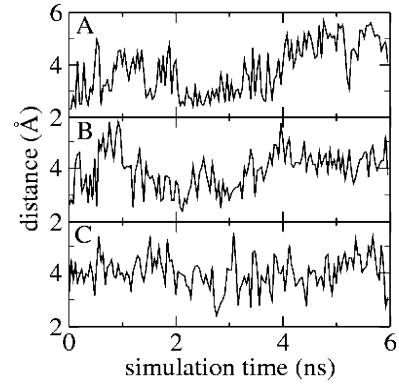

Figure 4. Distance between the oxygen atom of deprotonated Tyr28 and the *pro-S* hydrogen atom at C2 of the substrate DHQ as obtained from molecular dynamics simulation at 300 K. Panels A, B, and C show the distance for each of the three equivalent subunits of the DHQase trimer simulated.

3. Results

3.1. MD Simulation of Substrate-Bound DHQase (DHQ (E)). MD simulations of DHQase were carried out to investigate the structure and dynamics of the hydrogen bond network of the substrate bound state. The simulation of trimeric DHQase gives a stable protein structure as indicated by the small rmsd fluctuating between 1.5 and 1.8 Å relative to the crystallographic position of the trimer subunit in dodecameric DHQase. This shows that the simulation of an isolated trimer subunit does not cause any artificial conformational changes, thereby justifying our approach. The substrate DHQ is held tightly in the active site by about 20 hydrogen bonds formed with Ala81, Ala82, Arg117, Asn79, His85, His106, Ile107, Ser108, Tyr28, one crystallographic water molecule, and one to two further solvent molecules.

In the following, we discuss three regions of interest in more detail: First, the solvation structure of the deprotonated tyrosinate Tyr28; second, the solvation structure of the carbonyl oxygen atom of DHQ; and finally, the hydrogen-bonding network of the leaving group C1−OH. The tyrosinate anion is stabilized by formation of two strong hydrogen bonds with the guanidinium group of Arg113. The mean O···H hydrogen bond lengths are 2.06 and 2.16 Å, respectively. Additional stabilization is gained by hydrogen bond formation with solvent molecules. The water molecules in the channel connecting Tyr28 with the bulk solvent are very mobile, and the water molecule binding to Tyr28 is frequently replaced by a neighboring water molecule. The average distance between the tyrosinate oxygen atom and the proton at C2 is large, 3.81 (±) 0.94 Å, see Figure 4. The smallest distance observed for several configurations along the 6-ns trajectory was 2.3 Å. These events, which are coupled with the dynamics of hydrogen bond break/formation

Table 2. Free Energies Given in Kilocalories per Mole for the 10 QM Models Used in the Present Study[a,b]

	ΔΔG[a]	M1	M2	M3	M4	M5	M6	M6W	M7	M8	M8W
DHQ(aq)	-	3.1	3.1	3.1	3.1	3.1	3.1	3.1	3.1	3.1	3.1
DHQ(E)	0	0	0	0	0	0	0	0	0	0	0
TS1	-1.8	14.0	13.5	15.3	14.7	28.3	14.9	14.9	18.9	17.8	12.7
DHQ-O$^-$	0.3	12.3	12.2	14.6	14.6	11.3	13.4	13.5	14.5	13.2	8.5
TS2	-1.3	17.4	14.4	20.5	20.2	-	18.7	22.5	17.8	15.7	16.1
DHS(E)	-3.9	0.7	-4.2	9.2	8.0	-	-0.2	4.6	-5.9	-8.2	-3.3
DHS(aq)	-	2.2	2.2	2.2	2.2	2.2	2.2	2.2	2.2	2.2	2.2

[a] Gibbs free energy correction, which was calculated for a small unrestricted model of the DHQase active site and used in all models. [b] In the columns colored light green the charged Glu104 moiety is included, whereas in the columns colored light yellow the moiety is excluded or the charge is cancelled (M7). In the columns colored white a charged His67 is included in addition to the Glu104 moiety. The binding energy and the free energy of the reaction in aqueous solution are calculated from experimental equilibrium constants.[33,36]

between the oxyanion and solvent molecules, could eventually lead to deprotonation of the substrate. Thus, our simulations show that Tyr28 has sufficient conformational flexibility to overcome the relatively large separation distance between the deprotonated side chain oxygen and the C2-proton of the substrate (TyrO···C2 distance = 3.35 Å in the crystal structure 1GU1).

The carbonyl oxygen atom of DHQ forms on average two hydrogen bonds, one with a conserved crystal water and one with a solvent molecule. As was the case for Tyr28, the solvent molecule is very mobile and frequently gets replaced by another solvent molecule. The crystal water is tightly bound in the enzymatic pocket over the entire 6 ns of the present simulation. The side chain of Asn16 and the backbone atoms of Pro15 and Ala82 hold the crystal water in a rigid position. The hydrogen bond contacts between the substrate, crystal water, and the side chain of Asn16 could allow for the proposed proton transfer from Asn16 to the carbonyl oxygen atom after deprotonation of the substrate.

The hydrogen atom of the leaving group C1−OH forms a strong hydrogen bond with the carbonyl oxygen atom of Asn79 throughout the simulation. This ensures a correct orientation of the leaving group that eventually facilitates proton transfer from the Nδ of His106 to the oxygen atom of C1−OH. Thus, our molecular dynamics simulations show that the hydrogen bond network of substrate-bound DHQase is stable against thermal fluctuations. The general base Tyr28 and general acid His106 are connected to the bulk solvent via a chain of highly mobile water molecules that facilitate the shuffling of protons to and from the active site.

3.2. QM Calculations. The free energy profiles obtained from QM calculations of model systems M1−M8 are summarized in Table 2 and Figures 5 and 6 and are presented and discussed in the following sections.

Formation of Intermediate DHQ (E) → DHQ−Enolate. In the optimized structures of DHQ bound in the active site (M1−M8), the Tyr28 oxygen is located at a distance of 2.48−3.45 Å from the *pro-S* hydrogen of C2, and 3.39−4.39 Å from C2, in DHQ, respectively. The distance in the crystal structure corresponding to the latter is 3.35 Å, close to the lower values in the optimized range. The shorter distances were obtained for the larger models M6−M8, and especially in the models incorporating two additional waters (M6W and M8W) the distance approaches the experimental results. The transition state for proton transfer from C2 to the tyrosinate

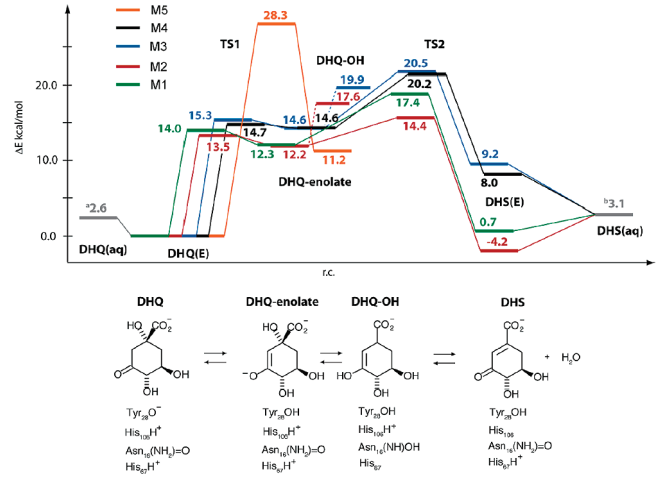

Figure 5. Computed energy profile for models M1−M5 for the reaction mechanism of type II DHQase. See Figure 2 for the models used. The apparent binding energy of DHQ in DHQase is $\Delta H_{app} = -2.6$ kcal/mol ($K_{app} = 5.40$ mM).[35] The standard enthalpy change of the overall reaction is $\Delta_r H^\circ_m = 0.55 \pm 0.55$ ($K = 4.6 \pm 1.5$).[32]

oxygen (TS1) is reached late, at an O−H bond distance of about 1.15 Å. The C2−C3 bond is shortened from 1.54 to 1.43 Å in TS1, indicating partial formation of a double bond. Very similar values for the C2−H distance (about 1.53 Å) are obtained for models M1−M8. Interestingly, the structure of TS1 is similar in all models even though the models differ substantially and M6−M8 are optimized in the gas phase.

The mean value of the free energy barrier for the proton transfer is 15.2 ± 2.0 kcal/mol, spanning values between 12.7 and 18.9 kcal/mol as obtained for M8W and M7, respectively. Note that the energies for M5 are excluded, since this model corresponds to the unfavorable assisted deprotonation mechanism discussed further below. If the models with the largest barriers are excluded (M7 and M8), the mean barrier is slightly smaller and the uncertainty is significantly reduced, 14.3 ± 0.9 kcal/mol. This value is in good agreement with the experimental rate-determining barrier of 13.4 kcal/mol, calculated from the turnover rate of 960 s^{-1} in wild-type *S. coelicolor* using transition-state theory. The barriers for M7 and M8 are too large because there is only the crystal water stabilizing the buildup of negative charge on the carbonyl oxygen atom. The second water molecule that, according to MD simulations, binds to

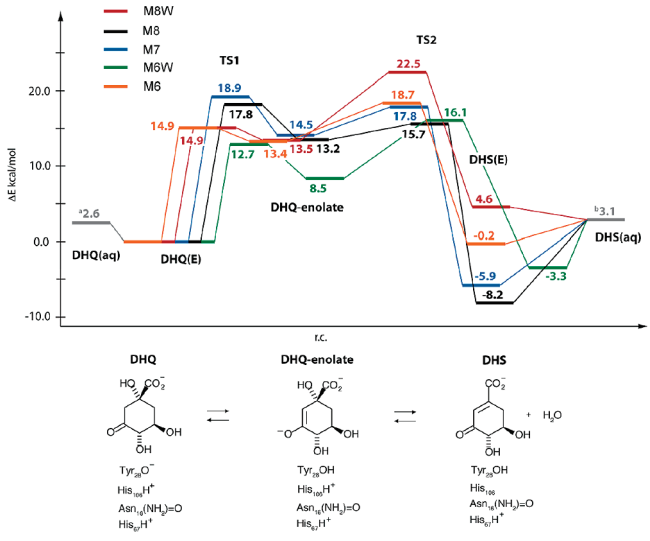

Figure 6. Computed energy profiles for models M6−M8 for the reaction mechanism of type II DHQase. See Figure 2 for the models used. The apparent binding energy of DHQ in DHQase is $\Delta H_{app} = -2.6$ kcal/mol ($K_{app} = 5.40$ mM).[36] The standard enthalpy change of the overall reaction is $\Delta_r H°_m = 0.55 \pm 0.55$ ($K = 4.6 \pm 1.5$).[33]

the carbonyl oxygen atom in the ES complex was not modeled. Indeed, inclusion of this second water molecule in model M8W reduces the barrier to a value consistent with the experimental rate. The smaller models M1−M4 give similarly good values as a consequence of two opposing effects. Both the water stabilizing deprotonated Tyr28 and the water stabilizing the buildup of negative charge in the transition state are not modeled. The effect is that the energies of reactant and transition state are raised by approximately equal amounts.

The formation of the enolate intermediate (DHQ−enolate) is endergonic with a mean value of 12.8 ± 1.9 kcal/mol, spanning from 8.5 to 14.6 kcal/mol for M8W and M3/M4, respectively. The deviation of model M8W from the mean value of the enolate intermediate is larger than for other models, and excluding M8W gives a mean value of 13.3 ± 1.2 kcal/mol. Thus, with the exception of M8W, the endergonicity of forming the enolate intermediate is less affected by the choice of the model then the preceding transition state. The endergonicity of this reaction step is the origin of the late transition state in TS1. The enolate intermediate is high in energy compared to $TyrO^-$, since there is no stabilization by a positively charged residue, such as Arg113 in the case of Tyr28. In M8W, the two extra water molecules modeled not only lower the barrier but also increase the stability of the enolate intermediate. During the reaction, the C3−O bond length of the carbonyl group is slightly increased, from 1.22 Å in DHQ to 1.25−1.30 Å in DHQ−enolate, whereas the C2−C3 bond is shortened from 1.51−1.52 to 1.38−1.44 Å. Interestingly, protonated Tyr28 remains hydrogen-bonded to the C2 atom of DHQ−enolate at a distance of 1.90 Å in models M1−M8, indicating that a significant part of the negative charge density remains on the C2 in the enolate intermediate. The corresponding distance in models M6W and M8W is 2.04−2.08 Å, indicating that more negative charge has been transferred to the oxygen atom in the models that contain the additional solvent molecule.

Isomerization of Intermediate DHQ−Enolate → DHQ−OH. As discussed above, the presence of a water molecule in the crystal structures together with solvent isotope effects indicate that two protons are involved in the rate-limiting step. This has led to the suggestion that an enol intermediate is formed instead of enolate. It has been suggested that the crystal water assists the proton transfer from Asn16 to the enolate, leaving Asn16 deprotonated.[16] However, such an intermediate was too high in energy to be plausible. Therefore, His67, which belongs to a neighboring subunit of the dodecamer structure of DHQase, was included in models M2−M5. A histidine residue is likely to be protonated at low cost at physiological pH and would thus be the most reasonable source of the proton needed to form the suggested enol intermediate. However, the formation of the enol through proton transfer from Asn16, which in turn is reprotonated by His67 to the isomeric form CNH(OH) of Asn16, is unfavorable according to our calculations. This enol intermediate is 5.4 and 5.3 kcal/mol higher in energy than the corresponding enolate intermediate in models M2 and M3, respectively. Note that the transition state leading to this state would be even higher in energy. Thus, the suggested enol intermediate does not seem likely to be of importance for the conversion of DHQ to DHS.

Formation of Product DHQ−Enolate → DHS (E) + H_2O. The second reaction step consists of protonation of the hydroxyl group at C1 by His106 and heterolytic cleavage of the C1−OH bond. This leads to the formation of the products, DHS and water. In the transition state TS2 the C1−OH bond distance is 1.67 Å for the smaller models M1−M5, which were optimized in a dielectric continuum. A significantly larger value of 1.95 Å was obtained for models M6−M8, which were optimized in the gas phase. Furthermore, the N−H bond of His106 increases from 1.06 Å in the enolate to 1.45 Å in TS2 for models M1−M5, and from 1.05−1.08 to 1.25 Å in models M6−M8. At the same time, the distance between the proton being transferred from His106 to the oxygen atom decreases from 1.62−1.63 to 1.09−1.10 Å in M1−M4 and from 1.54−1.69 to 1.19−1.27 Å in M6−M8. Tyr28 remains also in TS2 hydrogen bonded to C2. However, the hydrogen bond breaks upon formation of DHS.

The gas-phase-optimized structures are more affected by the presence of the charge on Glu104. The later transition states in the gas-phase models are caused by charge-transfer effects. After proton transfer from His106 to the DHQ−enolate, the His106-Glu104 motif is negatively charged, whereas the Tyr28-Arg113 motif is positively charged. The buildup of this net dipole is clearly disfavored in the gas phase when compared to a dielectric medium. Thus, the gas-phase models are optimized on a more endothermic energy surface, which leads to a later transition state consistent with Hammond's Postulate.[34,35] In addition to being an earlier transition state in the structure optimized in the dielectricum (M1−M4), the charge transfer is also closer to completion. The effect of the treatment of the surroundings on the reaction coordinates may seem to be large. However, the energy surface at the

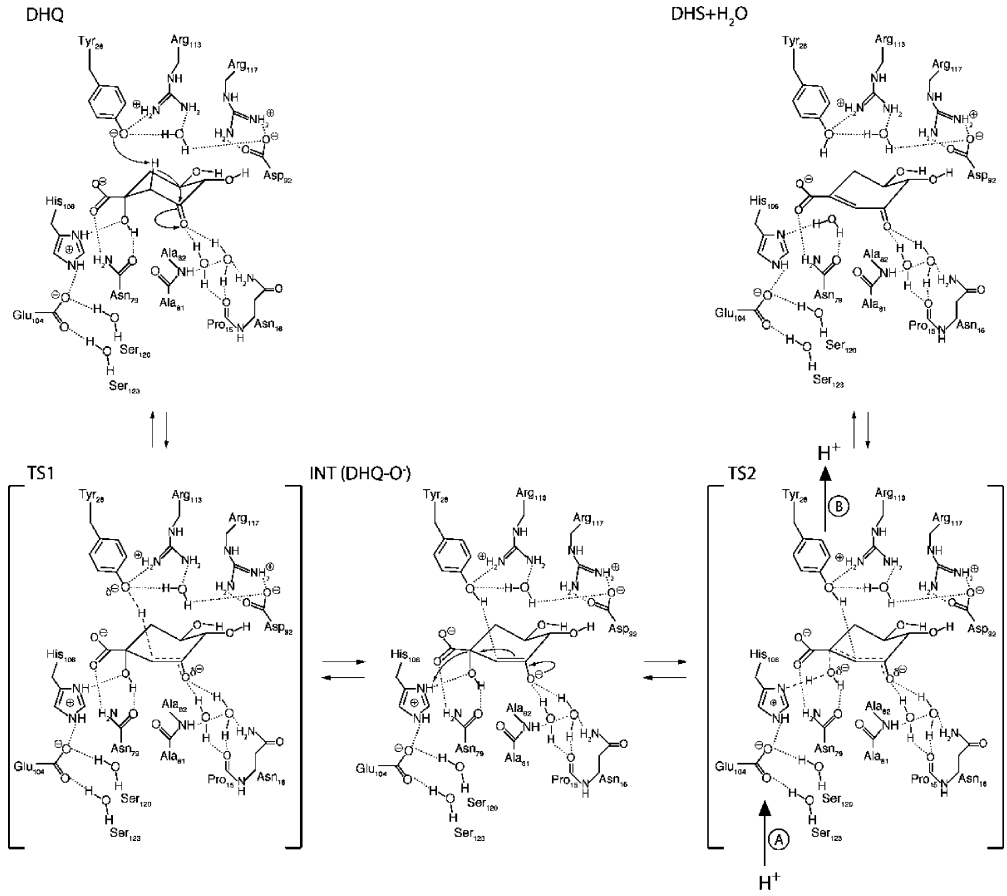

Figure 7. Revised mechanism for the dehydration of DHQ to DHS and water in DHQase. A and B indicate possible proton motions occurring before or connected to the transition state (TS2).

transition state TS2 is rather flat, and the effect on the barriers after the solvent effect has been added is rather small, as can be seen when comparing the energies for TS2 for the corresponding models (e.g., M4 and M6), displayed in Table 2. The barrier of TS2 is 5.0 ± 2.2 kcal/mol compared to that of the enolate intermediate and 18.1 ± 2.6 kcal/mol compared to that of DHQ, which is the resting state. The barrier for the different models ranges from 14.4 kcal/mol in M2 to 22.5 kcal/mol in M6W. This barrier should be compared to the experimental turnover rate of 960 s^{-1} in wild-type *S. coelicolor* corresponding to a rate-determining barrier of 13.4 kcal/mol.

The barrier for TS2 for most of the models is too high compared to that of experiment. However, as can be seen for models M2, M8, and M8W, the exclusion of Glu104 from the models leads to a reduced barrier height since a large part of the effect of the charge transfer and net dipole formation is removed. Thus, to reach a barrier height fitting well with experiment, a charge cancelation of Glu104 seems necessary. This could be realized by proton transfer through the hydrophilic channel connecting bulk solvent with Glu104. A similar effect would be obtained if Tyr28 were deprotonated at this stage and the catalytically active form of the active site regenerated. M7 has a somewhat higher barrier despite the protonated and thus uncharged Glu104. However, for this model larger structural changes occur, breaking the hydrogen bond between His106 and Glu104, causing the slightly higher barrier compared to that of M8.

The formation of the final products, enzyme-bound DHS and H_2O (DHS(E)), is exergonic by −13.7 ± 5.8 kcal/mol compared to the enolate intermediate and by 0.1 ± 6.1 kcal/mol compared to the enzyme−substrate complex DHQ(E), respectively. The overall reaction ranges from endergonic by 9.2 kcal/mol (M3) to exergonic by 8.2 kcal/mol (M8) (Table 2). This broad range of energy values is partly caused by the difference in charge-transfer effect due to the presence or absence of charged Glu104. A second cause is the difference in flexibility in the models. The structural changes in the last reaction step are large compared to those of previous steps. The smaller models, M1−M4, are much more restricted compared to models M6−M8 and will thus perform worse for the last step compared to the preceding stationary points. According to the experimental equilibrium constants for the reaction in aqueous solution and for substrate binding, unbound solvated DHS is 2.2 kcal/mol higher in energy compared to DHQ bound to the active site.

Kinetic Isotope Effects. As discussed above, solvent isotope studies imply that a different number of protons are involved in the rate-determining step for DHQases in different species. In *A. nidulans*, two protons take part in the rate-determining step, but only one in *M. tuberculosis*. One suggestion, which was shown to be energetically unfavored in the present study, involves the crystal water hydrogen bonding to the carbonyl group on C3 in DHQ. Another possibility could be that deprotonation of the substrate by Tyr28 does not occur directly but is assisted by a water molecule. In some species,

such as *A. nidulans*, water-assisted proton abstraction could occur, whereas in species such as *M. tuberculosis* no water molecule is involved. We investigated this possibility by adding an extra water molecule in model M5 and recalculating the energetics of the first reaction step. As can be seen in Table 2 and Figure 6, the extra water stabilizes the enolate intermediate, but the barrier for TS1 increased to 28.3 kcal/mol. Thus, the water-assisted proton transfer is unfavorable by 13.6 kcal/mol compared to direct proton transfer. This number is too large to explain the observed differences in solvent isotope effects for the different species. On a more speculative note, the solvent isotope effect could also be related to the proton transfer in or out of the active site before TS2 is reached. Further investigation is clearly needed to understand the kinetic differences among DHQases from different species.

4. Conclusions

The reaction mechanism of DHQase that results from our present theoretical investigation is illustrated in Figure 7. We find that deprotonated Tyr28 has enough conformational flexibility to overcome the large separation from the substrate in the crystal structure. The computed barrier for deprotonation of the substrate is in the range 13−15 kcal/mol, close to the experimental rate-limiting step corresponding to 13.4 kcal/mol. The deprotonation reaction follows a direct mechanism. The alternative, water-assisted, mechanism was found to be more than 10 kcal/mol higher in energy.

For the second reaction step, protonation of the enolate intermediate by His106 and water elimination, we find that a cancelation of the charge on Glu104 seems to be crucial for the reaction to proceed at a feasible rate. This could be accomplished by a proton entering the vicinity of Glu104, as an intermediate step in the regeneration of a protonated His106. A similar effect would probably be seen if the proton on Tyr28 is removed at this stage regenerating the catalytic tyrosinate. One could also imagine that this is coupled to the proposed motion of the loop covering the binding pocket, which may have to open upon product release.[15] The cancelation of charge on Glu104 before TS2, discussed above, would correspond to the first reaction step occurring in an environment best described by model M6W, while for the second reaction step the surroundings are best described by model M8W.

The mechanism shown in Figure 7 is, to a certain extent, similar to a previously proposed mechanism based on crystal structure analysis and kinetic data.[16] However, one important difference concerns the nature of the intermediate. The formation of an enol form of the intermediate was suggested in ref 16 to explain the solvent isotope effects of the enzyme-catalyzed reaction. Our calculations indicate, however, that the enol form is significantly higher in energy than the corresponding enolate form, showing that the enol intermediate should not be of importance for the reaction studied.

Our suggestion that shuffling of protons is needed to pass TS2 could also have implications on the interpretation of the solvent isotope effects. If the proton motions and the breaking of the C1−O bond in TS2 are tightly coupled, the proton motions may be affecting the solvent isotope effects. Different species may exhibit slightly different energetics for the proton motions, which could give rise to the differences observed for the number of protons involved in the rate-limiting step. This would also suggest that the second reaction step is rate-limiting.

Previous and present proposals for the reaction mechanism of type II DHQase assume that Tyr28 is deprotonated. If the reaction is initiated by deprotonation of the C2 atom, then there is indeed little doubt that tyrosinate is the catalytic base. This is simply because there are no other basic residues in the vicinity of the C2 proton. In future investigations, we aim at computing the pK_a value of this residue using a novel QM/MM technique. Moreover, we would like to compute the acidity constants of a number of other catalytic residues along the reaction path to corroborate and extend our present findings.

Acknowledgment. We thank the Wenner-Gren Foundations and Swedish Research Council for postdoctoral funding (L.M.B.), Unilever for funding (J.B.O.M.), the European Commission for an EST PhD studentship under the Marie Curie Actions Program (M.M.), and the Royal Society for a University Research Fellowship (J.B.). We thank the U.K.'s EPSRC National Service for Computational Chemistry Software for providing us with both access to software and computer time. We also thank Prof. Chris Abell for valuable discussions on type II DHQase.

Appendix

Model M0. The M0 model for the first reaction step (formation of enolate of DHQ) includes DHQ with a protonated carboxyl group (mimicking the stabilization given by the carboxyl binding pocket), Tyr28 modeled as phenolate, and a water molecule hydrogen bonding to the carbonyl oxygen atom of DHQ. In the second reaction step (formation of DHS and water), the phenolate molecule was removed and His106, modeled as protonated imidazole, was included.

Models M1−M5. The active site models are illustrated in Figure 2. The carboxylate binding pocket, which consists of Ile107 and Ser108, is modeled by three water molecules, mimicking the hydrogen bonds from the backbone peptides and OH side chain of Ser108. Furthermore, His85, which accepts a hydrogen bond from the OH group on C5 in DHQ, is also modeled as water molecules. The salt bridge between Arg117 and Asp92 is modeled as a formate ion and an ammonium ion, respectively. Tyr28 was cut between C_α and C_β, and Arg113 was cut between C_γ and C_δ. A crystal water molecule, which was observed in several X-ray structures of DHQase, was proposed to assist a proton transfer from Asn16 to the enolate form of DHQ, forming the corresponding enol intermediate. Because of the suggested importance of this intermediate, a larger part of the protein around the crystal water was included in the model. This water molecule can form three hydrogen-bonding contacts to surrounding residues. Hydrogen bonds can be formed to the amide group of Asn16, the backbone carbonyl of Pro15, and the backbone amide of Ala82. The backbone amide of Ala82 was modeled as formamide, and the carbonyl group of Pro15 as an acetate group forming a peptide bond with full side chain model of

Asn16. Furthermore, His67 was included in the model since the proposed deprotonation of Asn16 was shown to be energetically unfavorable. Furthermore, the proximity of His67 together with a plausible pK_a of around 7 make the latter a reasonable candidate for the presence of an extra proton in the system, which could stabilize a DHQ enol intermediate. His67 is modeled as imidazole. His106 is modeled as a protonated imidazole, and Glu104 is modeled as a formate ion. Ser120 and Ser123, which both are hydrogen bonding to Glu104, are modeled as water molecules. Asn79 is modeled as formamide.

The smallest model M1 differs from M3 by the exclusion of all residues that form hydrogen bonds to the crystal water, which is hydrogen bonding to the carbonyl oxygen atom of DHQ. In model M2, the Glu104-Ser120-Ser123 part of the active site is excluded. In model M3 His67 is protonated, whereas in model M4 it is deprotonated. In model M5, an additional water molecule is included, bridging Tyr28 and the carbonyl oxygen on C3, and later taking part in the proton transfer from DHQ to Tyr28.

Models M6−M8. For models M6−M8, an attempt was made to include all of the protein in the vicinity of the substrate. Model M6W, which consists of about 230 atoms, is shown schematically in Figure 2. The N-terminal end of peptide chain His106-Ile107-Ser108-Asn109-Ile110 was cut at the C_α−N bond between His106 and Val105. Similarly, the C_α−C(=O) bond between Ile110 and His111 at the C-terminal end was cut. Furthermore, only the backbone of Asn109 was included, and the side chain, which is pointing away from the active site, was excluded. In the peptide chain discussed above, every second C_α was restricted in the optimization with the coordinates taken from the X-ray structure (1GU1), starting with C_α in His106. The full side chain including the C_α was included in the model of Tyr28, whereas the C_α−N and C_α−C(=O) bonds to Ile27 and Gly29, respectively, were cut. Arg113 was cut between C_β and C_γ. The model of Arg117 is equivalent to the model of Arg113. Asp92 was cut between C_α and C_β. Pro15 and Asn16 were modeled as the full side chain of Asn16 and include the peptide bond to Pro15, whereas the C(=O)−C_α in Pro15 and C_α−C(=O) bond in Asn16 were cut. Ala81 is modeled as the full residue forming peptide bonds to both Ala82 and Pro80, in which the C_α−C(=O) bonds were cut. Asn79 was cut between C_α and C_β. His85 was modeled as an imidazole ring cutting the C_α−C_β bond. Glu104 was cut between C_β and C_γ. Ser120 and Ser123 were modeled as water molecules, cutting the C_β−O(H) bonds. Moreover, a varying number of water molecules were included in the models. First, the crystal water molecule that stabilizes the enolate intermediate and that forms hydrogen bonds to Pro15, Asn16, and Ala82 in a number of crystal structures was included in all models. In M6, M7, and M8, a second water molecule was added by doubly protonating an oxygen atom of a buffer molecule (tartaric acid) that was resolved in the proximity of the active site. Model M7 is equivalent to M6 except that Glu104 is protonated in the former. In model M8, Glu104 and the two hydrogen-bonding water molecules modeling Ser120 and Ser123 are excluded. In the MD simulations, Tyr28 forms hydrogen bonds to Arg113 and to a water molecule. Furthermore, the carbonyl oxygen on C3 in DHQ is, in addition to the conserved water, hydrogen bonding to at least one more water molecule. Accordingly, we added two more water molecules in models M6W and M8W, which otherwise are identical to M6 and M8. One is hydrogen bonding to Tyr28 and is positioned in between the water molecule present in model M6 and Tyr28 (Figure 2). The second water molecule is hydrogen bonding to the carbonyl oxygen on C3 in DHQ and to the carbonyl in Pro15.

References

(1) Herrmann, K. M. The shikimate pathway as an entry to aromatic secondary metabolism. *Plant Physiol.* **1995**, *107*, 7.

(2) Herrmann, K. M. The shikimate pathway: Early steps in the biosynthesis of aromatic compounds. *Plant Cell* **1995**, *7*, 907.

(3) Herrmann, K. M.; Weaver, L. M. The shikimate pathway. *Annu. Rev. Plant Physiol. Plant Mol. Biol.* **1999**, *50*, 473.

(4) Schmid, J.; Amrhein, N. Molecular organization of the shikimate pathway in higher plants. *Phytochemistry* **1995**, *39*, 737.

(5) Steinrücken, H. C.; Amrhein, N. The herbicide glyphosate is a potent inhibitor of 5-enolpyruvyl-shikimic acid-3-phosphate synthase. *Biochem. Biophys. Res. Commun.* **1980**, *94*, 1207.

(6) Gourley, D. G.; Shrive, A. K.; Polikarpov, I.; Krell, T.; Coggins, J. R.; Hawkins, A. R.; Isaacs, N. W.; Sawyer, L. The two types of 3-dehydroquinase have distinct structures but catalyze the same overall reaction. *Nat. Struct. Biol.* **1999**, *6*, 521.

(7) Shneier, A.; Harris, J.; Kleanthous, C.; Coggins, J. R.; Hawkins, A. R.; Abell, C. Evidence for opposite stereochemical courses for the reaction catalysed by type I and type II dehydroquinases. *Bioorg. Med. Chem. Lett.* **1993**, *3*, 1399.

(8) Chaudhuri, S.; Duncan, K.; Graham, L. D.; Coggins, J. R. Identification of the active-site lysine residues of two biosynthetic 3-dehydroquinases. *Biochem. J.* **1991**, *275*, 1.

(9) White, P. J.; Young, J.; Hunter, I. S.; Nimmo, H. G.; Coggins, J. R. The purification and characterization of 3-dehydroquinase from *Streptomyces coelicolor*. *Biochem. J.* **1990**, *265*, 735.

(10) Moore, J. D.; Lamb, H. K.; Garbe, T.; Servos, S.; Dougan, G.; Charles, I. G.; Hawkins, A. R. Inducible overproduction of the *Aspergillus nidulans* pentafunctional AROM protein and the type-I and -II 3-dehydroquinases from *Salmonella typhi* and *Mycobacterium tuberculosis*. *Biochem. J.* **1992**, *287*, 173.

(11) Robinson, D. A.; Stewart, K. A.; Price, N. C.; Chalk, P. A.; Coggins, J. R.; Lapthorn, A. J. Crystal structures of *Helicobacter pylori* type II dehydroquinase inhibitor complexes: New directions for inhibitor design. *J. Med. Chem.* **2006**, *49*, 1282.

(12) Kleanthous, C.; Deka, R.; Davis, K.; Kelly, S. M.; Cooper, A.; Harding, S. E.; Price, N. C.; Hawkins, A. R.; Coggins, J. R. A comparison of the enzymological and biophysical properties of two distinct classes of dehydroquinase enzymes. *Biochem. J.* **1992**, *282*, 687.

(13) Harris, J. M.; Gonzalez-Bello, C.; Kleanthous, C.; Hawkins, A. R.; Coggins, J. R.; Abell, C. Evidence from kinetic isotope studies for an enolate intermediate in the mechanism of type II dehydroquinases. *Biochem. J.* **1996**, *319*, 333.

(14) Price, N. C.; Boam, D. J.; Kelly, S. M.; Duncan, D.; Krell, T.; Gourley, D. G.; Coggins, J. R.; Virden, R.; Hawkins, A. R. The folding and assembly of the dodecameric type II dehydroquinases. *Biochem. J.* **1999**, *338*, 195.

(15) Maes, D.; Gonzalez-Ramirez, L. A.; Lopez-Jaramillo, J.; Yu, B.; De Bondt, H.; Zegers, I.; Afonina, E.; Garcia-Ruiz, J. M.; Gulnik, S. Structural study of the type II 3-dehydroquinate dehydratase from *Actinobacillus pleuropneumoniae*. *Acta Crystallogr., Sect. D: Biol. Crystallogr.* **2004**, *60*, 463.

(16) Roszak, A. W.; Robinson, D. A.; Krell, T.; Hunter, I. S.; Fredrickson, M.; Abell, C.; Coggins, J. R.; Lapthorn, A. J. The structure and mechanism of the type II dehydroquinase from *Streptomyces coelicolor*. *Structure* **2002**, *10*, 493.

(17) Frederickson, M.; Parker, E. J.; Hawkins, A. R.; Coggins, J. R.; Abell, C. Selective inhibition of type II dehydroquinases. *J. Org. Chem.* **1999**, *64*, 2612.

(18) Frederickson, M.; Roszak, A. W.; Coggins, J. R.; Lapthorn, A. J.; Abell, C. (1*R*,4*S*,5*R*)-3-Fluoro-1,4,5-trihydroxy-2-cyclohexene-1-carboxylic acid: The fluoro analogue of the enolate intermediate in the reaction catalyzed by type II dehydroquinases. *Org. Biomol. Chem.* **2004**, *2*, 1592.

(19) Kerbarh, O.; Bulloch, E. M.; Payne, R. J.; Sahr, T.; Rébeillé, F.; Abell, C. Mechanistic and inhibition studies of chorismate-utilizing enzymes. *Biochem. Soc. Trans.* **2005**, *33*, 763.

(20) Payne, R. J.; Peyrot, F.; Kerbarh, O.; Abell, A. D.; Abell, C. Rational design, synthesis, and evaluation of nanomolar type II dehydroquinase inhibitors. *ChemMedChem* **2007**, *2*, 1015.

(21) Toscano, M. D.; Payne, R. J.; Chiba, A.; Kerbarh, O.; Abell, C. Nanomolar inhibition of type II dehydroquinase based on the enolate reaction mechanism. *ChemMedChem* **2007**, *2*, 101.

(22) Berman, H. M.; Westbrook, J.; Feng, Z.; Gilliland, G.; Bhat, T. N.; Weissig, H.; Shindyalov, I. N.; Bourne, P. E. The protein data bank. *Nucleic Acids Res.* **2000**, *28*, 235.

(23) Seminario, J. M. Calculation of intramolecular force fields from second-derivative tensors. *Int. J. Quantum Chem.* **1996**, *60*, 1271.

(24) Essmann, U.; Perera, L.; Berkowitz, M. L.; Darden, T.; Lee, H.; Pedersen, L. G. A smooth particle mesh Ewald method. *J. Chem. Phys.* **1995**, *103*, 8577.

(25) Becke, A. D. Density-functional thermochemistry. III. The role of exact exchange. *J. Chem. Phys.* **1993**, *98*, 5648.

(26) Lee, C.; Yang, W.; Parr, R. G. Development of the Colle-Salvetti correlation-energy formula into a functional of the electron density. *Phys. Rev. B* **1988**, *37*, 785.

(27) Frisch, M. J.; Trucks, G. W.; Schlegel, H. B.; Scuseria, G. E.; Robb, M. A.; Cheeseman, J. R.; Montgomery, J. A., Jr.; Vreven, T.; Kudin, K. N.; Burant, J. C.; Millam, J. M.; Iyengar, S. S.; Tomasi, J.; Barone, V.; Mennucci, B.; Cossi, M.; Scalmani, G.; Rega, N.; Petersson, G. A.; Nakatsuji, H.; Hada, M.; Ehara, M.; Toyota, K.; Fukuda, R.; Hasegawa, J.; Ishida, M.; Nakajima, T.; Honda, Y.; Kitao, O.; Nakai, H.; Klene, M.; Li, X.; Knox, J. E.; Hratchian, H. P.; Cross, J. B.; Bakken, V.; Adamo, C.; Jaramillo, J.; Gomperts, R.; Stratmann, R. E.; Yazyev, O.; Austin, A. J.; Cammi, R.; Pomelli, C.; Ochterski, J. W.; Ayala, P. Y.; Morokuma, K.; Voth, G. A.; Salvador, P.; Dannenberg, J. J.; Zakrzewski, V. G.; Dapprich, S.; Daniels, A. D.; Strain, M. C.; Farkas, O.; Malick, D. K.; Rabuck, A. D.; Raghavachari, K.; Foresman, J. B.; Ortiz, J. V.; Cui, Q.; Baboul, A. G.; Clifford, S.; Cioslowski, J.; Stefanov, B. B.; Liu, G.; Liashenko, A.; Piskorz, P.; Komaromi, I.; Martin, R. L.; Fox, D. J.; Keith, T.; Al-Laham, M. A.; Peng, C. Y.; Nanayakkara, A.; Challacombe, M.; Gill, P. M. W.; Johnson, B.; Chen, W.; Wong, M. W.; Gonzalez, C.; Pople, J. A. Gaussian 03, revision C.02; Gaussian, Inc.: Wallingford, CT, 2004.

(28) Cancès, E.; Mennucci, B.; Tomasi, J. A new integral equation formalism for the polarizable continuum model: Theoretical background and applications to isotropic and anisotropic dielectrics. *J. Chem. Phys.* **1997**, *107*, 3032.

(29) Cossi, M.; Barone, V.; Mennucci, B.; Tomasi, J. Ab initio study of ionic solutions by a polarizable continuum dielectric model. *Chem. Phys. Lett.* **1998**, *286*, 253.

(30) Mennucci, B.; Tomasi, J. Continuum solvation models: A new approach to the problem of solute's charge distribution and cavity boundaries. *J. Chem. Phys.* **1997**, *106*, 5151.

(31) Blomberg, M. R. A.; Siegbahn, P. E. M.; Babcock, G. T. Modeling electron transfer in biochemistry: A quantum chemical study of charge separation in *Rhodobacter sphaeroides* and photosystem II. *J. Am. Chem. Soc.* **1998**, *120*, 8812.

(32) Curtiss, L. A.; Raghavachari, K.; Redfern, P. C.; Pople, J. A. Assessment of Gaussian-3 and density functional theories for a larger experimental test set. *J. Chem. Phys.* **2000**, *112*, 7374.

(33) Tewari, Y. B.; Goldberg, R. N.; Hawkins, A. R.; Lamb, H. K. A thermodynamic study of the reactions: {2-dehydro-3-deoxy-arabino-heptanoate 7-phosphate(aq)=3-dehydroquinate(aq) + phosphate(aq)} and {3-dehydroquinate(aq)=3-dehydroshikimate(aq) + H_2O(l)}. *J. Chem. Thermodyn.* **2002**, *34*, 1671.

(34) Hammond, G. S. A correlation of reaction rates. *J. Am. Chem. Soc.* **1955**, *77*, 334.

(35) Leffler, J. E. Parameters for the description of transition states. *Science* **1953**, *117*, 340.

(36) Krell, T.; Horsburgh, M. J.; Cooper, A.; Kelly, S. M.; Coggins, J. R. Localization of the active site of type II dehydroquinases. Identification of a common arginine-containing motif in the two classes of dehydroquinases. *J. Biol. Chem.* **1996**, *271*, 24492.

(37) Case, D. A.; Darden, T. A.; Cheatham, T. E., III; Simmerling, C. L.; Wang, J.; Duke, R. E.; Luo, R.; Merz, K. M.; Pearlman, D. A.; Crowley, M.; Walker, R. C.; Zhang, W.; Wang, B.; Hayik, S.; Roitberg, A.; Seabra, G.; Wong, K. F.; Paesani, F.; Brozell, S.; Tsui, V.; Gohlke, H.; Yang, L.; Tan, C.; Mongan, J.; Hornak, V.; Cui, G.; Beroza, P.; Mathews, D. H.; Schafmeister, C.; Ross, W. S.; Kollman, P. A. AMBER9 University of California, San Francisco, 2006.

(38) Phillips, J. C.; Braun, R.; Wang, W.; Gumbart, J.; Tajkhorshid, E.; Villa, E.; Chipot, C.; Skeel, R. D.; Kale, L.; Schulten, K. Scalable molecular dynamics with NAMD. *J. Comput. Chem.* **2005**, *1781*, 26.

CT800480D